Reconstruction of Thermal Signals in Infrared Images Reveals Temperature Perturbations during Full Forearm Occlusion

by W.M. Liu*, K. Chang**, S. Yoon**, and A.M. Gorbach**

*Department of CSEE, National Chung Cheng University, Taiwan; *wmliu@cs.ccu.edu.tw*
**Infrared Imaging and Thermometry Unit, National Institute of Biomedical Imaging and Bioengineering,
 National Institutes of Health, 9000 Rockville Pike, Building 13, Bethesda, MD 20892, USA;
 gorbacha@mail.nih.gov

Abstract

Assessment of peripheral blood flow may allow the prediction of cardiovascular disease. Thermal Signal Reconstruction and the *k-means* algorithm were applied to infrared images of the volar aspect of a subject's forearm collected during full occlusion of blood flow, revealing segments of subcutaneous vessels that increased and decreased temperature during the occlusion. Comparisons of infrared-derived maps of the forearm and near-infrared images of veins in the forearm showed that the heat diversity co-localized with veins and venous valves.

1. Introduction

Non-invasive measurement of skin blood flow is useful in helping to assess the delivery of oxygen and nutrients, and has multiple clinical applications in peripheral vascular disease, surgery, and management of wound healing. Although various techniques exist to visualize superficial blood flow (capillaroscopy, laser Doppler flowmetry, laser speckle contrast), infrared imaging (IR) provides the advantage of being able to access cutaneous and subcutaneous vessels simultaneously via perfused perforator vessels. Arterial blood at core temperature is warmer than the exposed skin surface, which has been cooled by radiant losses, evaporation, and contact with room air. Therefore, local microvascular blood flow, originating from the core, can be used as an endogenous, natural thermal contrast agent for IR visualization of the skin vessels, and IR may serve as a surrogate measure of tissue perfusion [1, 2, 3]. In the current study, we used IR imaging of the human forearm without thermal contrast, during occlusion and non-occlusion of arterial and venous blood flow.

Several methods have been proposed to highlight the thermal discontinuities during the heat transfer process, such as pulse phase thermography [4], principal component thermography [5], high order statistics [6], and thermal signal reconstruction (TSR) [7, 8]. These methods are mainly used to locate defects in non-destructive testing (NDT) applications widely used in materials science. Although the term 'defect' is not directly applicable to IR imaging of human vasculature, the contrast between vessels and surrounding areas might be enhanced with the use of these methods.

In our previous study, the TSR technique was applied to the reperfusion period after full arterial occlusion [1]. The release of cuff pressure created an impulse of thermal energy brought by the restoration of blood flow, which is analogous to the original experimental scenario of TSR in NDT. TSR may not seem as applicable to the occlusion period due to the lack of an initial impulse of thermal energy. However, it is important to note that the cooling process from the lack of blood flow is very similar to the air-cooling of the testing material in NDT after the initial thermal impulse. We hypothesize that our modified TSR analysis can be effective in enhancing spatial and temporal heterogeneity of thermal changes during the forearm occlusion period.

2. Methods
2.1. IR Imaging

We analyzed IR images of the forearm of a healthy 23-year old male subject. The IR camera (3.0–5.0 μm wavelength, 0.015°C temperature resolution) was positioned 42 cm above the forearm. The subject's arm was placed on a padded armrest at heart level with the volar aspect facing upward toward the camera. Prior to the start of IR imaging, three triangular thermo-reflective pieces of tape were placed on the skin as fiducial markers, and the subject was given a 20 min period of acclimatization to the room temperature. In total, 3600 IR images (640×512 pixels each) were collected continuously (2 Hz acquisition rate) over the 35 min reactive hyperemia test that consisted of a 15 min baseline period, a 5 min occlusion period, and a 15 min reperfusion period. The IR images were then saved as an image cube for subsequent offline analysis. Full occlusion was achieved with an automatic pressure cuff (moorVMS-PRES, Moor Instruments, Inc., USA) inflated to 200 mmHg.

2.2. Vein Imaging

Fifteen images collected with a near-infrared vein imager (VeinViewer, Christie, USA) were combined to create a single composite vein map of the forearm. The near-infrared vein imager is composed of an array of light-emitting diodes that produces near-infrared light at a peak wavelength of 760 nm. Near-infrared light at a wavelength of 760 nm is absorbed by hemoglobin present in venous blood vessels, while the surrounding subcutaneous tissue reflects it. A camera that is sensitive to near-infrared wavelength in the vein imager captures the reflected photons, forms the

resulting image, and a video projector subsequently casts a real-time vein image onto the skin surface. The veins appear as dark lines and the skin appears fluorescent green (figure 1a). As claimed in [9], veins can be visualized as deep as 10 mm from the surface of the skin. The following functional test was utilized to detect vein valve locations: 1) Selected vein segments were visualized via real-time projection vein images onto the skin area (figure 1a). 2) Blood from a visualized vein segment was flushed out by the application of localized pressure (via fingertip) on the subject's skin, moving from the proximal to distal direction (figure 1b). 3) Each junction of a region with venous blood refilling and a region without venous blood refilling was marked as a valve on the composite vein map (figure 1c).
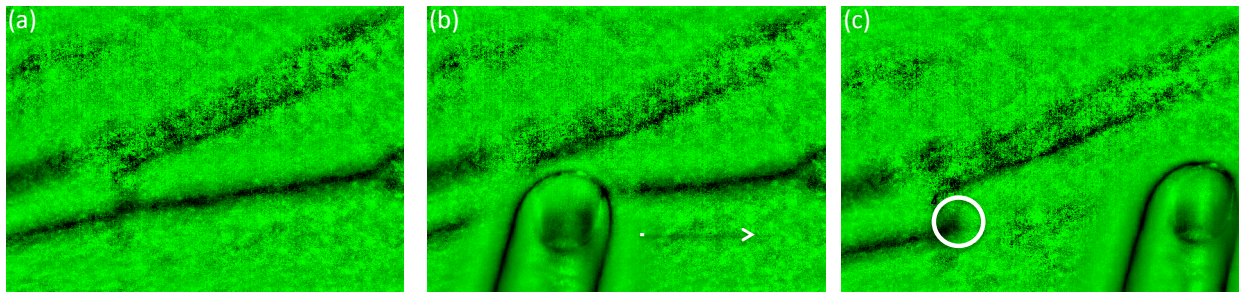
Fig. 1. *Example of valve location detection. (a) Projected image of vein segment (black) visualized with the vein imager. (b) Application of localized pressure via fingertip on vein of interest followed by flushing of blood from the proximal to distal direction (white arrow). (c) Valve location overlaid as a white circle.*

2.3. IR Image Processing
2.3.1 Image Alignment

Three regions of interest (ROI) representing fiducial markers were manually circumscribed in MATLAB (MathWorks, Inc., USA) and were used to correct for translational motion of the forearm. By using the 1st IR image during the 5 min occlusion as the reference, the rest of the 3599 collected images were then aligned using a rigid body registration technique [2, 10].

2.3.2 Thermal Signal Reconstruction

The TSR technique used polynomial fitting to approximate the raw IR images in logarithmic time-temperature scale. Such parameterized approximation was then used to calculate the 1st derivative images. When TSR is used solely to show the map of defect locations, reference [11] suggests to use only 4th or 5th degree polynomial to generate derivative images with larger heterogeneity). However, since a 9th degree polynomial fitting created less distortion in terms of temporal thermal dynamics, we applied this setting to calculate 600 1st derivative TSR images and also 600 2nd derivative TSR images. The contrast of each 1st derivative TSR image was estimated by the BN's contrast algorithm [1, 3] to compare with the proposed method for image synthesis.

2.3.3 K-means Cluster Algorithm with Short Time Series (STS) Distance Measure

The *k-means* algorithm [12] iteratively clusters the scattered data into *k* centroids. In the study, the parameter *k* was estimated by the Signal Subspace Estimation (SSE) technique [2, 13] to be equal to 13 (*k* = 13). For data consisting of multiple time profiles, *k-means* assigns each of the time profiles to the closest time profile cluster. We followed the same rationale of [2] and used STS distance [14] instead of Euclidean distance as the similarity measurement. The *k-means* algorithm (*k* = 13) was applied to both the 600 raw IR images and the 600 1st derivative TSR images during occlusion.

2.3.4 Calculation of Total Temperature Decrease and Total Temperature Increase

To measure the extent of temperature change during the occlusion period, Total Temperature Decrease and Total Temperature Increase were calculated for each pixel in the forearm as follows: 1) TSR processing was applied to the raw IR time-temperature profile to calculate both the TSR signal (figure 2b) and the corresponding 1st derivative signal (figure 2c). 2) All zero crossings of the 1st derivative TSR signal were located, dividing the occlusion period into multiple time windows (vertical red lines in figure 2). Within these time windows, it was noted that a positive 1st derivative indicates that temperature is increasing, while a negative 1st derivative indicates that temperature is decreasing. 3) For time windows undergoing temperature decrease, the area between the maximum temperature within that time window and the temperature curve was calculated (figure 2d). 4) The Total Temperature Decrease was then defined as the sum of each calculated area for every time window undergoing temperature decrease. 5) For time windows undergoing temperature increase, the area between the temperature curve and the minimum temperature within that time window was calculated (figure 2d). 6) The Total Temperature Increase was defined as the sum of each calculated area for every time window undergoing temperature increase.
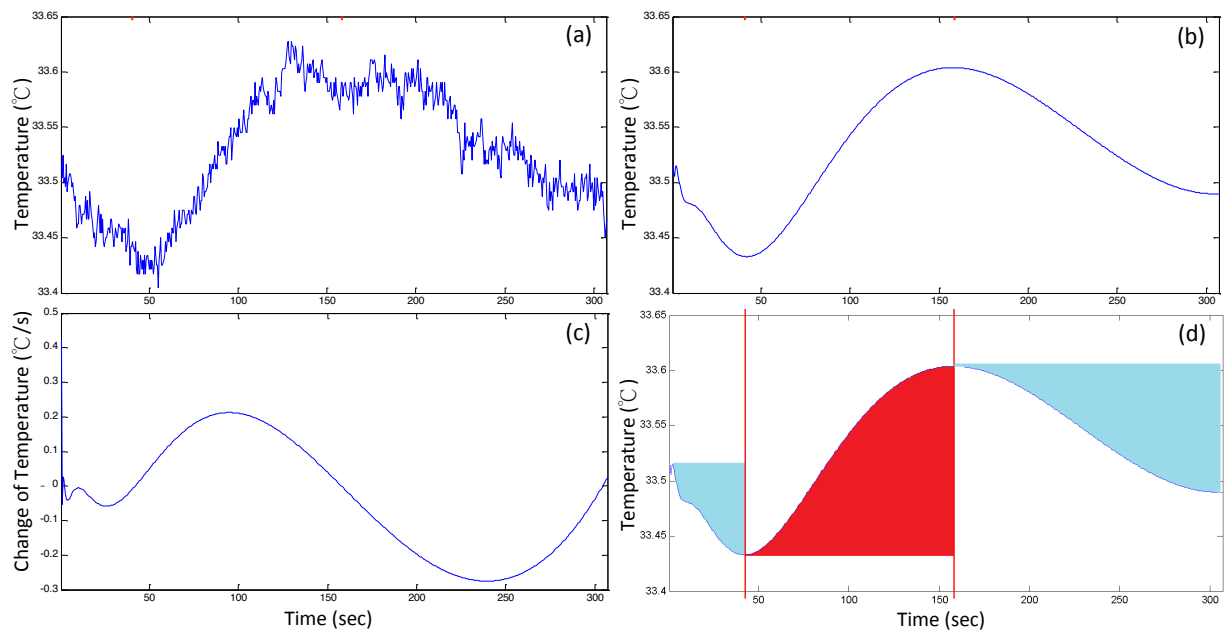
Fig. 2. *Calculation of Total Temperature Decrease and Total Temperature Increase for a representative ROI during the occlusion period. (a) Raw IR temperature vs. time profile during the 5 min occlusion. (b) TSR signal. (c) 1st derivative TSR signal. Note that the zero-crossings from the 1st derivative TSR signal are marked as vertical red lines in the four plots, dividing the occlusion period into three time windows. (d) TSR signal with the shaded red area representing the Total Temperature Increase, and the sum of the two shaded light blue areas representing the Total Temperature Decrease.*

3. Results
3.1. Contrast Between Vessels and Surrounding Tissue is Highly Dynamic

To show the limitation of looking at individual frames of the 1st derivative TSR images, BN's contrast of each 1st derivative image was plotted with respect to time during occlusion (figure 3). Different patterns within the 1st derivative TSR images were observed over time (figures 3b-d), resulting in a highly dynamic contrast (figure 3a).
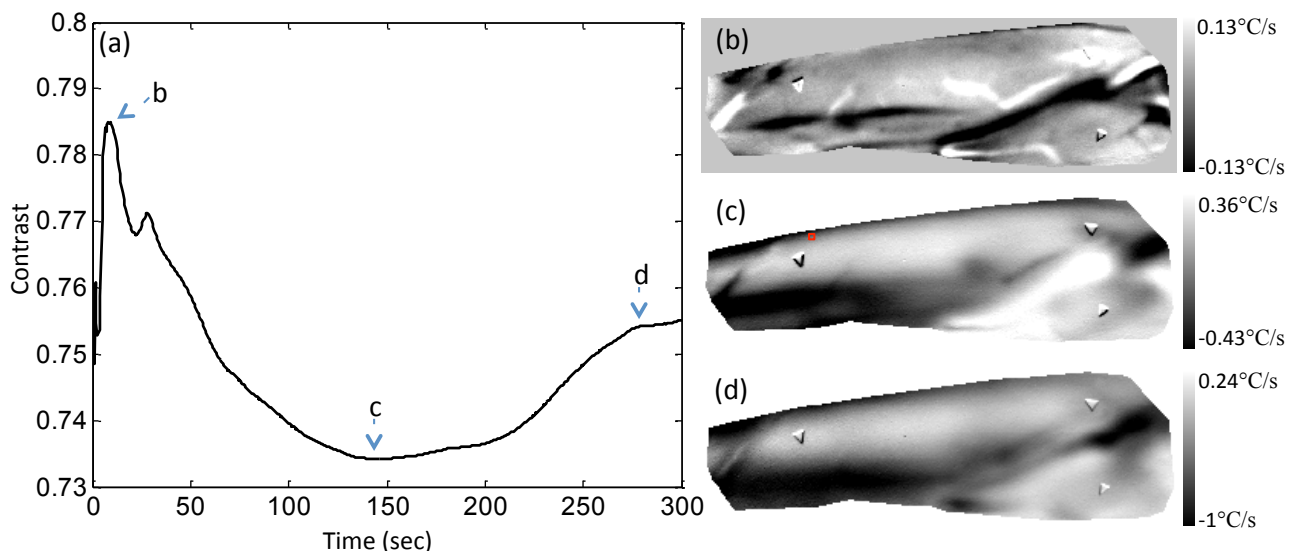
Fig. 3. *(a) A plot of BN's contrast value vs. time calculated during the 5 minute of occlusion. The contrast is calculated within a ROI shown by the red rectangle in (c). Three 1st derivative TSR images (b, c, d) for different time points are shown.*

3.2. Heating and Cooling During Occlusion

Different ROIs revealed temporal heterogeneity reflecting time windows of heating and cooling (figure 4a). Specifically, the blue ROI (figure 4b) showed a constant decrease in temperature (figures 4a and 5, blue), the red ROI (figure 4b) showed immediate increase followed by decrease in temperature (figures 4a and 5, red), and the magenta ROI (figure 4b) showed a delayed increase followed by decrease in temperature (figures 4a and 5, magenta).
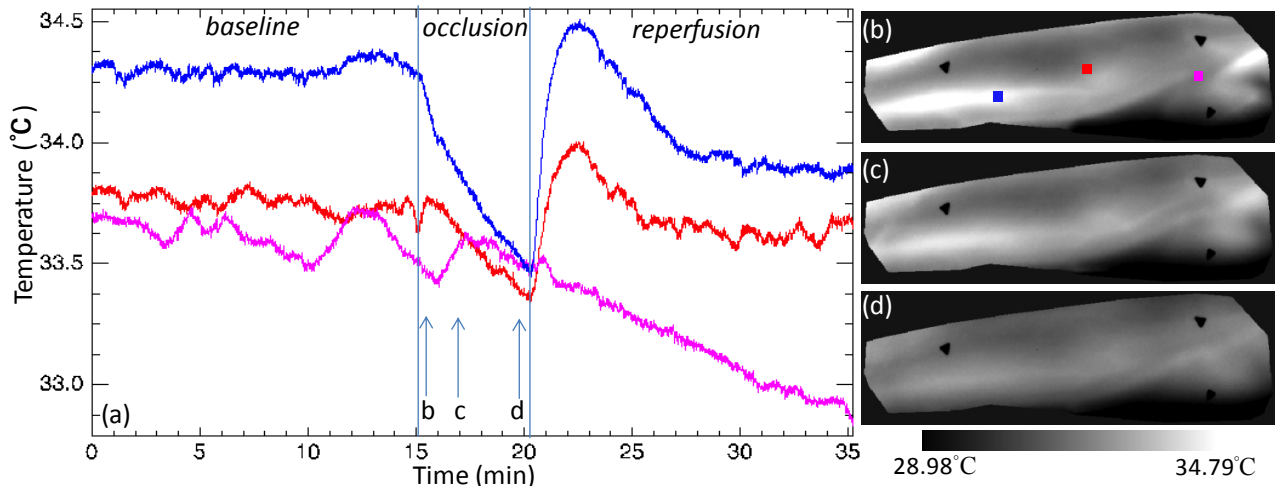
Fig. 4. *(a) A plot of temperature vs. time calculated for the 15 min baseline, 5 min occlusion, and 15 min of reperfusion periods for the three ROIs in (b). The raw IR images (b, c, d) were collected at 8, 87, 286 s after the start of occlusion, respectively (b, c, d in figure 4a). The fiducial markers appear as three dark triangles on the raw IR images (b, c, d).*
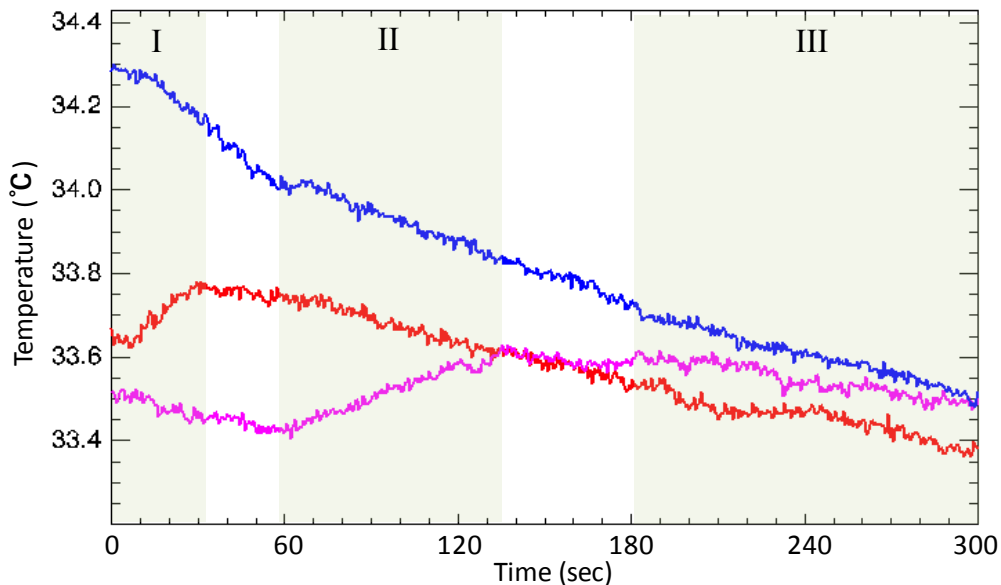
Fig. 5. *Temperature vs. time profile during occlusion period (extracted from figure 4a and zoomed for clarity). The temperature of the red ROI increased during 1-32 s (time window I). The temperature of the magenta ROI increased during 57-135 s (time window II). The temperature of all three ROIs showed decrease in temperature during 180-300 s (time window III).*

The 2nd derivative of the TSR signals revealed further temporal differences in heating and cooling during occlusion. Specifically, the magenta ROI had highly dynamic 2nd derivative values compared to the red and blue ROIs (figure 6b).
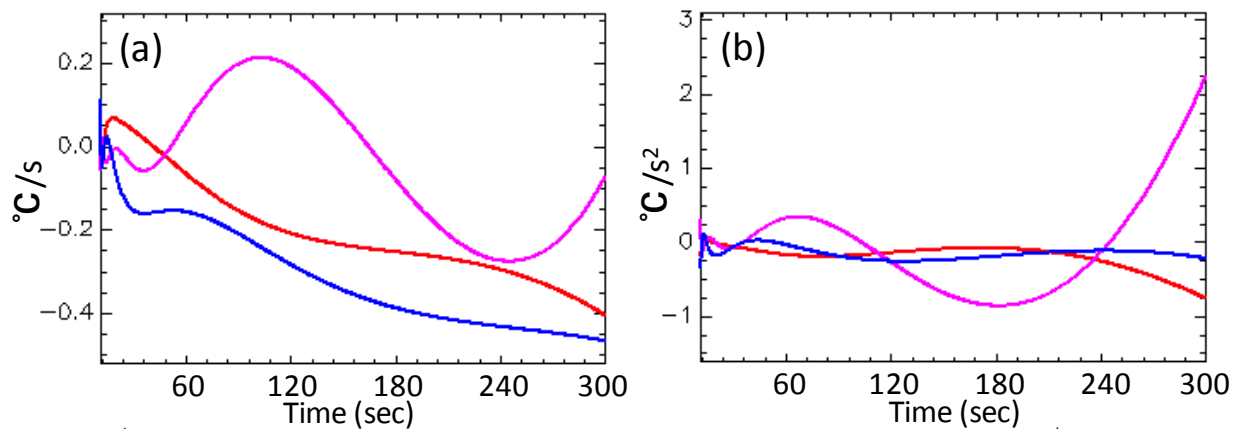
Fig. 6 *(a) 1st derivative of TSR signal reconstruction during occlusion of the ROIs in figure 3b. (b) 2nd derivative of TSR signal reconstruction.*

3.3 Application of *k-means* Algorithm to Raw IR and 1st Derivative TSR Images

To classify temperature responses based on their similarity, the *k-means* algorithm was applied to raw IR images. The resulting classification map showed 13 diffuse clusters with no apparent vascular pattern (figure 7a). The *k-means* algorithm was then applied to the 1st derivative TSR image series, which showed an apparent vascular pattern in the resulting classification map (figure 7b).
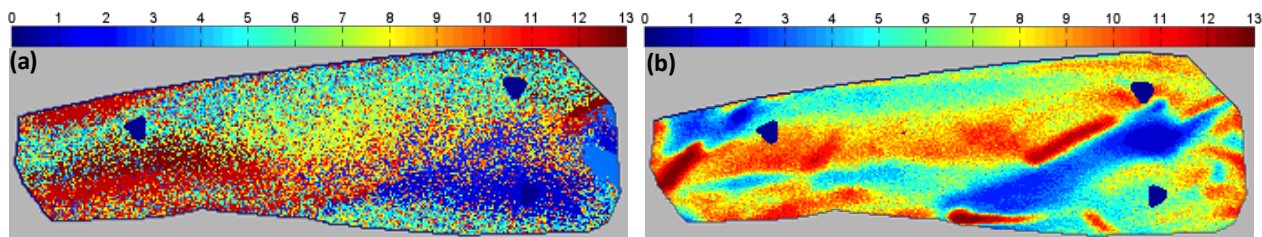
Fig. 7. *Classification map of k-means clustering (k = 13 derived from the SSE technique) for (a) raw IR images and (b) 1st derivative TSR images. A different color indicates each of the 13 classes. The class number 0 belongs to fiducial markers that were excluded from analysis.*

3.4 Total Temperature Increase and Decrease Maps Reveal Spatial and Temporal Heterogeneity

Total Temperature Increase maps (figures 8a-d) and Total Temperature Decrease maps (figure 9a-d) were calculated for different time windows (time windows I, II, III in figure 5). The results showed temporal and spatial heterogeneity in heating and cooling. Specifically, vein segments showed a high Total Temperature Increase during early stages of occlusion (figures 8a, b) and no temperature increase during late stages of occlusion (figure 8c).
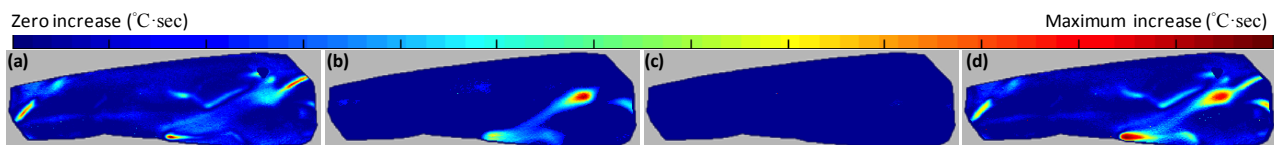
Fig. 8. *Total Temperature Increase from (a) 1-32 s, (b) 60-135 s, (c) 180-300 s, and (d) 1-300 s.*
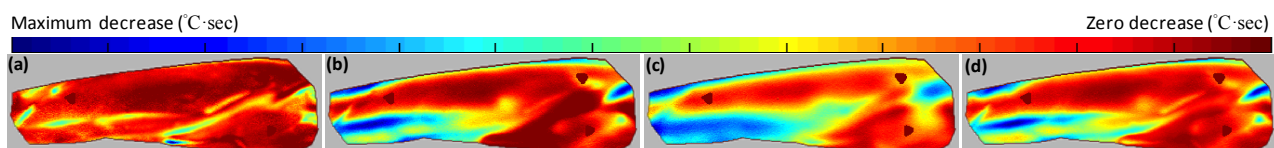
Fig. 9. *Total Temperature Decrease from (a) 1-32 s, (b) 60-135 s, (c) 180-300 s, and (d) 1-300 s.*

Notice, a large vein (figure 8a, blue) showed the greatest Total Temperature Decrease (figure 9b and d, blue).

3.5 Areas with Total Temperature Increase Co-localized with Venous Valve Locations

The locations of the vein segments and subsequent venous valves were determined by combining real-time near-infrared imaging and functional test, as described in section 2.2. In total, 18 valves within vein segments were identified (figure 10b).
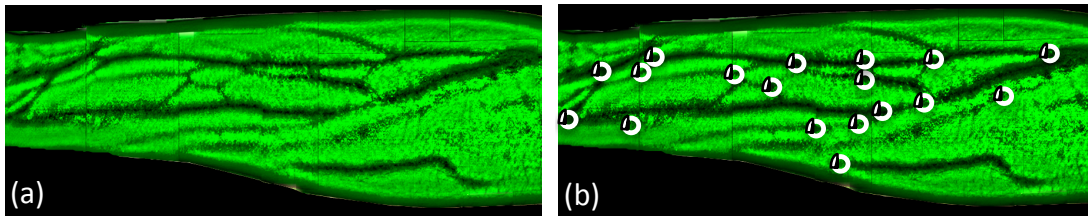
Fig. 10. *(a) Composite vein image of the volar aspect of the forearm. (b) Composite vein image of the volar aspect of the forearm with all detected valves (overlaid as white circles).*

Among the 18 valves identified, valves 1-6 (figure 11a) co-localized with regions that had a high Total Temperature Increase (figure 11c-d). Specifically, these valves are distal to vein segments that display high Total Temperature Increase during occlusion.

Comparison of valve locations (figure 11a) with the classification map (figure 11b) showed co-localization of valves with veins identified via class 1 (valves 2 and 6), class 9 (valve 3), and class 13 (valves 1, 4, and 5), as defined in figure 7.
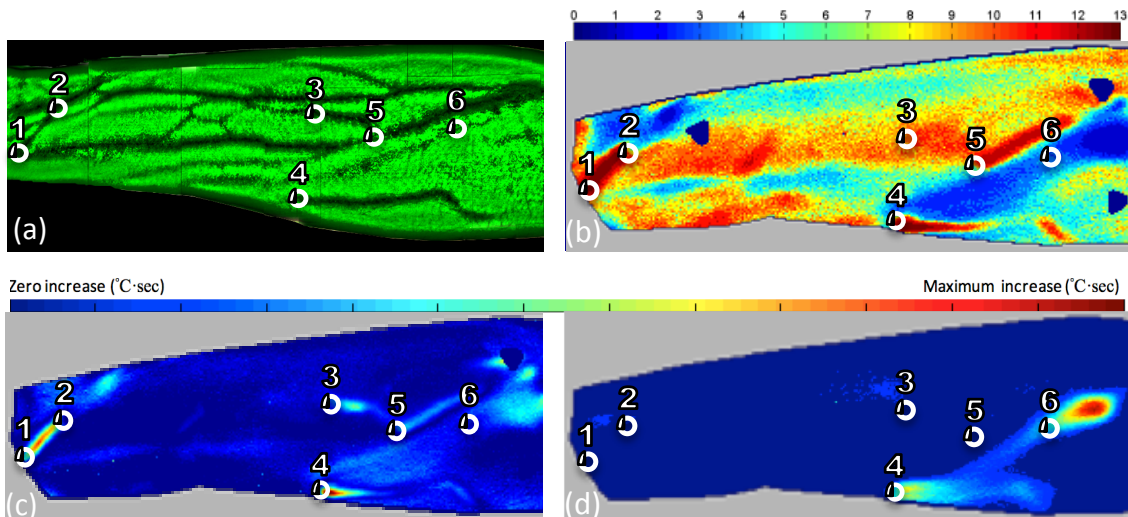
Fig. 11. *(a) Composite vein image displaying six specific venous valves which co-localized with high Total Temperature Increase segments on maps (c-d). (b) Classification map of k-means clustering for 1st derivative TSR image with the six venous valves overlaid. Total temperature increase maps for (c) 1-32 s and for (d) 60-135 s time windows with the six venous valves overlaid.*

4. Discussion

In this study, TSR processing was applied to a 5 min occlusion period to enhance vasculature that is otherwise not apparent in the raw IR images. The contrast in the 1st derivative TSR images was shown to be highly dynamic over time. As a result, the overall temperature changes during occlusion cannot be represented by a single 1st derivative TSR image.

To identify differences in temperature dynamics, the *k-means* algorithm was applied to the 1st derivative TSR signal reconstruction images to identify 13 classes that displayed distinct temperature patterns. Because the application of only the *k-means* algorithm to the raw IR images did not show the vascular pattern (figure 7a), the application of both TSR and *k-means* algorithms (figure 7b) is justifiable.

The venous patterns revealed by 1) the classification map of k-means clustering for 1st derivative TSR signal reconstruction and 2) the Total Temperature Increase maps were validated through comparisons to a venous and valve map. Co-localization of valves and regions with high Total Temperature Increase during occlusion was observed.

The observed time-varying diversity of temperature during occlusion suggested various blood flow perturbations in spite of full vascular occlusion of the forearm. Specifically, rapid temperature increases occuring 1-32 s after occlusion) may reveal low resistance vessels that have an influx of blood due to the mechanical forces of the pressure cuff and subsequent displacement of blood. Delayed temperature increase (occuring 60-135 s after occlusion) may indicate blood

redistribution originating from deeper vessels to the surface. Tissue hypoxia and vasodilator metabolites dilate arterioles and decrease vascular resistance during occlusion [15]. In both rapid and delayed cases of temperature increase, valves may prevent retrograde flow in veins, which causes warm blood that enters a segment to be retained. It was found that a large vein displayed the highest Total Temperature Decrease during occlusion (figure 9b-c). Large decreases in temperature may be due to large veins having greater surface area for conductive cooling than other vessels.

It was shown that certain regions of the forearm displayed a relatively constant 2nd derivative, while other regions displayed a dynamic 2nd derivative. This finding shows that even during complete occlusion of the forearm, there are also fluctuations in the rates of heating and cooling. Heat retention within the forearm during tissue ischemia might be modulated by processes (which have not been extensively studied) occurring during states of oxygen depletion, redistribution of blood flow and extracellular liquids, and/or residual (post-occlusion) thermogenesis.

5. Conclusions

Applying TSR and *k-means* to IR images collected during full forearm occlusion can be used to reveal subcutaneous vessels and their functional heterogeneity. Our analysis showed existence of both heating and cooling processes during full forearm occlusion.

The vein architecture revealed by IR images was validated through comparisons with a vein and venous valve map created through near-infrared imaging. We observed co-localization of Total Temperature Increase during occlusion and venous valve location.

6. Acknowledgements

REFERENCES

[1] Liu W.M., Maivelett J., Kato G.J., Taylor VI J.G., Yang W.C., Liu Y.C., Yang Y.G., Gorbach A.M., "Reconstruction of thermographic signals to map perforator vessels in humans". Quantitative Infrared Thermography Journal, vol. 9, pp. 123-133, 2012.

[2] Liu W.M., Meyer J., Scully C.G., Elster E., Gorbach A.M., "Observing temperature fluctuations in humans using infrared imaging". Quantitative Infrared Thermography Journal, 2011, vol. 8, pp. 21-36, 2012.

[3] Beghdadi A., Negrate A.L., "Contrast enhancement technique based on local detection of edges". Computer Vision, Graphics, and Image Processing, vol. 46, pp. 162-174, 1989.

[4] Gorbach A.M., Heiss J., Kufta C., Sato S., Fedio P., Kammerer W.A., Solomon J., Oldfield E.H., "Intraoperative infrared functional imaging of human brain". Ann Neurol, vol. 54, pp. 297-309, 2003.

[5] Gorbach A. M., Ackerman H., Liu W., Meyer J., Littel P., Seamon C., Footman E., Chi A., Zorca S., Krajewski M., Cuttica M., Machado R., Cannon 3rd R., and Kato G., "Infrared imaging of nitric oxide-mediated blood flow in human sickle cell disease". Microvasc Res, vol. 84, pp. 262-269, 2012.

[6] Maldague X., Marinetti S., "Pulse Phase Infrared Thermography". J. Appl. Phys., vol. 79, pp. 2694-2698, 1996.

[7] Shepard S., Lhota J., Rubadeux B., Rubadeux B.A., Wang D., Ahmed T., "Reconstruction and enhancement of active thermographic image sequences". Opt. Eng., vol. 42, pp. 1337-1342, 2003.

[8] Rajic, N., "Principal Component Thermography for Flaw Contrast Enhancement and Flaw Depth Characterization in Composite Structures". Composite Structures, vol. 58, pp. 521–528, 2002.

[9] Strehle, E. M., "Making the invisible visible: near-infrared spectroscopy and phlebotomy in children". Telemedicine and e-Health, vol. 16, pp. 889-893, 2010.

[10] Frackowiak R.S.J., Ashburner J.T., Penny W.D., Zeki, S., Friston K.J., Frith C.D., Dolan R.J., Price C.J., "Human brain function". Academic Press, London, 1997.

[11] Roche J.M., Leroy F.H., and Balageas D.L., "Images of Thermographic Signal Reconstruction Coefficients: A Simple Way for Rapid and Efficient Detection of Discontinuities". Materials evaluation, pp. 73-78, 2014.

[12] MacQueen, J. B., "Some methods for classification and analysis of multivariate observations". Berkeley Symp on Math. Statist and Prob, United States of America (Berkeley), 1967.

[13] Dias, J., Nascimento, J., "Estimation of signal subspace on hyperspectral data". Geoscience and Remote Sensing Symposium, Spain (Barcelona), 2007.

[14] Möller-Levet C.S., Klawonn, F., Cho K.H., Wolkenhauer O., "Fuzzy clustering of short time series and unevenly distributed sampling points". Proceedings of the 5th International Symposium on Intelligent Data Analysis, Germany (Berlin), 2003.

[15] Selvaraj, N., et al. "Monitoring of reactive hyperemia using photoplethysmographic pulse amplitude and transit time". Journal of Clinical Monitoring and Computing, vol. 23, pp. 315-322, 2009.